

Class 23 (04/15/24)

Lienard-Wiechert Potentials for Moving Point Charges



Review Key Results Potentials

- Maxwell's Equations with sources $\rho(\mathbf{r},t)$ and $\mathbf{j}(\mathbf{r},t)$

$$\nabla \cdot \vec{E} = \frac{\rho}{\epsilon_0}, \quad \nabla \times \vec{E} = -\frac{\partial \vec{B}}{\partial t}, \quad \nabla \cdot \vec{B} = 0, \quad \nabla \times \vec{B} = \mu_0 \vec{j} + \mu_0 \epsilon_0 \vec{E}$$

- With $\vec{E} = -\nabla V - \frac{\partial \vec{A}}{\partial t}$ and $\vec{B} = \nabla \times \vec{A}$

- Inhomogeneous Wave Equations for $V(\mathbf{r},t)$ and $\mathbf{A}(\mathbf{r},t)$

- Solutions are the Retarded Potentials

$$V(\vec{r}, t) = \frac{1}{4\pi\epsilon_0} \int_{V'} \frac{\rho(\vec{r}', t-r)}{|\vec{r}-\vec{r}'|} dV', \quad \mathbf{A}(\vec{r}, t) = \frac{\mu_0}{4\pi} \int_{V'} \frac{\vec{A}(\vec{r}', t-r)}{|\vec{r}-\vec{r}'|} dV'$$



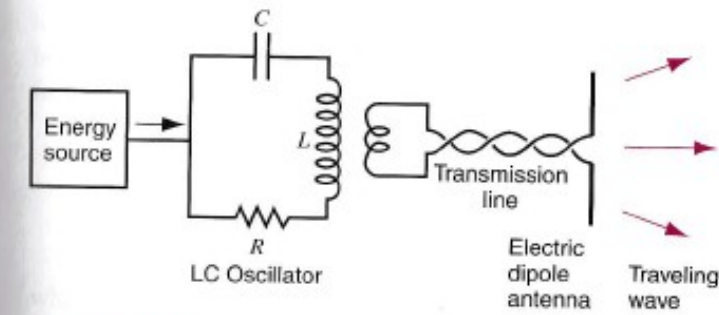


FIGURE 38-5. An arrangement for generating a traveling electromagnetic wave.

Electric dipole radiation

$$\text{oscillating charge } q(t) = q_0 \cos(\omega t)$$

$$\text{oscillating current } i(t) = \frac{dq}{dt}$$

Potentials:

$$V(r, \theta, t) = \underbrace{\frac{P_0 \cos \theta}{4\pi \epsilon_0} \left(-\frac{\omega}{c} \right)}_{\text{far away from the dipole}} \underbrace{\frac{\sin[\omega(t - r/c)]}{r}}_{\text{radiation field potential}} + \underbrace{\frac{P_0 \cos \theta \cos[\omega(t - r/c)]}{4\pi \epsilon_0 r^2}}_{\text{near field } (\propto \frac{1}{r^2}) \text{ potential}}$$

far away from the dipole

near-field static potential

$$\vec{A}(r, \theta, t) = -\frac{\mu_0 P_0 \omega}{4\pi} \frac{\sin[\omega(t - r/c)]}{r} (\cos \theta \hat{r} - \sin \theta \hat{\theta})$$

in the vicinity of the electric dipole



Radiation fields:

Spherical waves

$$\vec{E} = -\vec{\nabla}V - \frac{\partial \vec{A}}{\partial t} = -\frac{\mu_0 P_0 \omega^2}{4\pi} \left(\frac{\sin\theta}{r}\right) \cos[\omega(t - \tau/c)] \hat{\theta}$$

$$\vec{B} = \vec{\nabla} \times \vec{A} = -\frac{\mu_0 P_0 \omega^2}{4\pi c} \left(\frac{\sin\theta}{r}\right) \cos[\omega(t - \tau/c)] \hat{\phi}$$

Calculate $\vec{s}(\vec{r}, t) = \frac{1}{\mu_0} (\vec{E} \times \vec{B})$, $\langle S \rangle$, $\langle P \rangle$

At large distances from the dipole, the observer of the approaching spherical wave "sees" a plane wave front because of the large radius of curvature.



$$\vec{S}(\vec{r}, t) = \frac{1}{\mu_0} (\vec{E} \times \vec{B}) = \frac{\mu_0}{c} \left\{ \frac{P_0 \omega^2}{4\pi} \frac{\sin \theta}{r} \cos [\omega(t - r/c)] \right\} \hat{y}^2 \hat{r}$$

$$\text{Time average } \langle \vec{S} \rangle = \frac{\mu_0 P_0^2 \omega^4}{32\pi^2 c} \frac{\sin^2 \theta}{r^2}$$

$$\langle P \rangle = \int \langle \vec{S} \rangle \cdot d\vec{a} = \frac{\mu_0 P_0^2 \omega^4}{2\pi c}$$



Today's Topic: Lienhard-Wiechert Potentials

- The solutions to the inhomogeneous wave equation for electric potential $V(r, t)$ and magnetic potential $A(r, t)$ in the case of point charges q moving at velocity v are the Lienhard-Wiechert potentials.
- Next class, Lienhard-Wiechert potentials will be utilized to calculate the electromagnetic fields radiated by moving point charges.



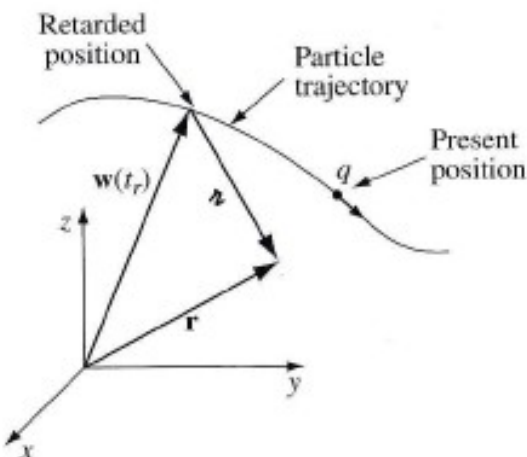
Lienhard-Wiechert Potentials

$$V(\vec{r}, t) = \frac{1}{4\pi\epsilon_0} \frac{qc}{|\vec{F} - \vec{F}'|c - (\vec{F} - \vec{F}') \cdot \vec{v}}$$

$$\vec{A}(\vec{r}, t) = \frac{\mu_0}{4\pi} \frac{qc\vec{v}}{(|\vec{F} - \vec{F}'|c - (\vec{F} - \vec{F}') \cdot \vec{v})^2} = \frac{\vec{v}}{c^2} V(\vec{r}, t)$$

q : magnitude of point charge , \vec{v} : velocity of the
point charge
 c : speed of light

\vec{F} : vector to field point , $(\vec{F} - \vec{F}')$: vector from
retarded position to
field point





Seismograph developed by Emil Wiechert

Emil Johann Wiechert (1861 – 1928) was a physicist and geophysicist who made many contributions to both fields, including presenting the first verifiable model of a layered structure of the Earth and being among the first to discover the electron. He went on to become the world's first Professor of Geophysics at the University of Göttingen.
https://en.wikipedia.org/wiki/Emil_Wiechert



Alfred Liénard (1869-1958), Engineer (Mining)
Professor, École des mines de Saint Étienne,
Director l'École des mines, Paris (1929-1936).
President of the Mathematical Society in France.



His students drew cartoons of Alfred Lienhard.
More are here:

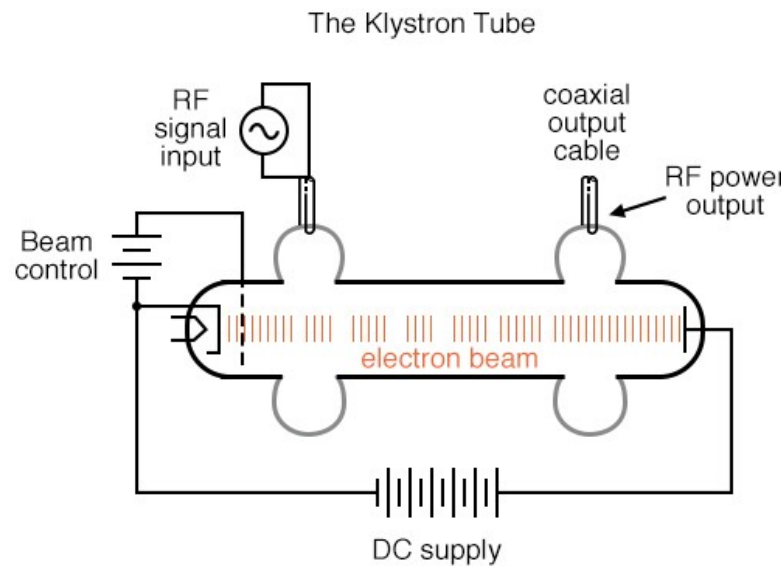
https://en.wikipedia.org/wiki/Alfred-Marie_Li%C3%A9nard

<http://www.annales.org/archives/x/lienard.html>



Why are Lienhard-Wiechert Potentials relevant?

- Moving point charges are important sources or amplifiers of electromagnetic radiation with properties tailored to specific applications.
- Example: Microwave Tubes (Klystrons, Magnetrons, etc.)



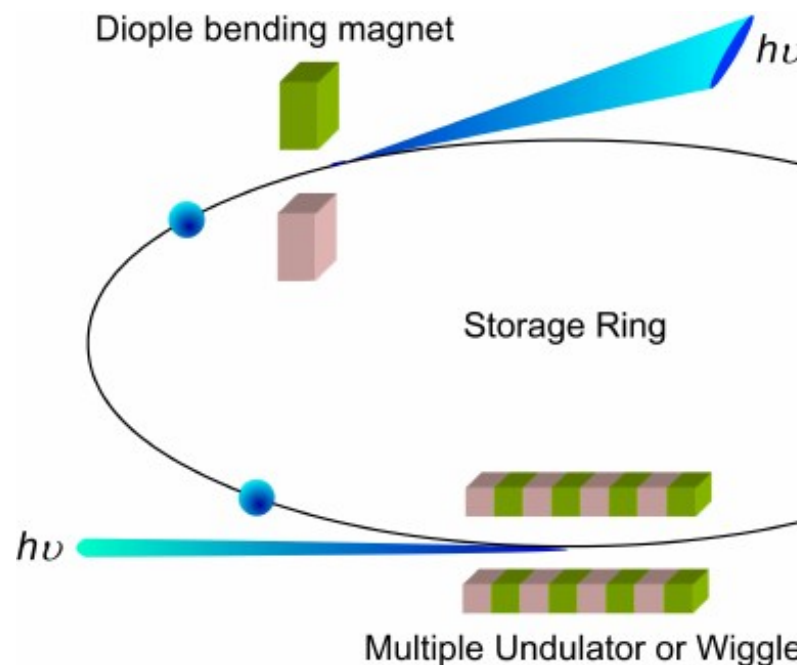
Global Market for
Microwave Tubes 2019:
US \$1140 Million.



Electromagnetic Radiation of Moving Point Charges is Used for Research



National Synchrotron Light Source II (NSLS-II) at Brookhaven National Laboratory is one of the newest, most advanced synchrotron facilities in the world and a U.S. Department of Energy (DOE) Office of Science User Facility.



Accelerated electrons radiate electromagnetic waves !

- Linear acceleration: electron speeds up (\mathbf{a} and \mathbf{v} parallel)
- Centripetal acceleration : electron moves with constant velocity on a circular path (\mathbf{a} perpendicular to \mathbf{v})



Electric & magnetic field of a moving point charge : (derived from Lienhard-Wiechert Potentials)

acceleration
↓

$$\vec{E}(\vec{r}, t) = \frac{q}{4\pi\epsilon_0} \frac{\vec{F} - \vec{F}'}{((\vec{F} - \vec{F}') \cdot \vec{u})^3} \left[(c^2 - v^2) \vec{u} + (\vec{r} - \vec{r}') \times (\vec{u} \times \vec{a}) \right]$$

q: charge, \vec{v} : velocity of charge, \vec{F} : vector to field point

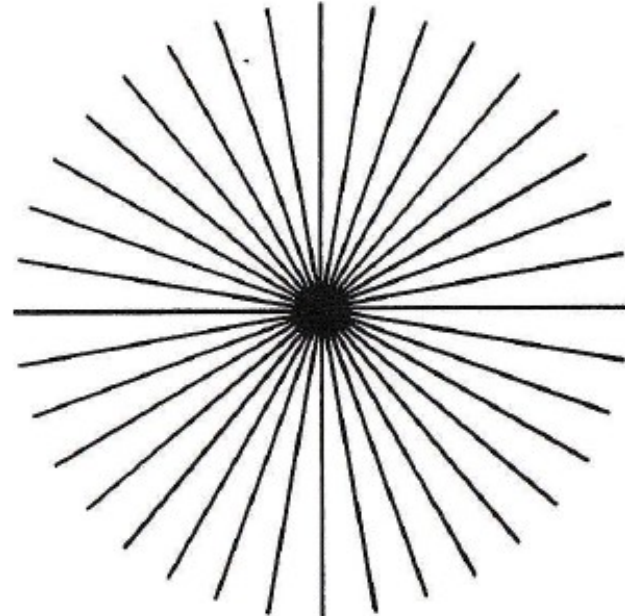
c: speed of light, $(\vec{F} - \vec{F}')$: vector from retarded position

to field point, and $\vec{u} = c \left(\frac{\vec{F} - \vec{F}'}{|\vec{F} - \vec{F}'|} \right) - \vec{v}$

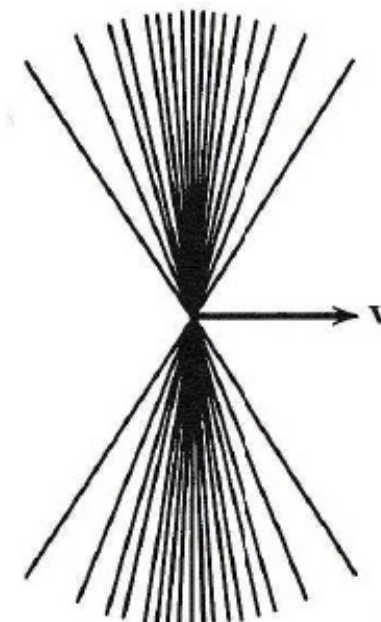
$$\vec{B}(\vec{r}, t) = \frac{1}{c} \frac{\vec{F} - \vec{F}'}{|\vec{F} - \vec{F}'|} \times \vec{E}(\vec{r}, t)$$



Coulomb fields



(a)



(b)

Coulomb field of point charge at rest

Coulomb field of point charge moving at velocity v for v approaching the speed of light c , E is transverse to direction of motion



Single-Shot Electron-Beam Bunch Length Measurements

I. Wilke

Universität Hamburg, Institut für Angewandte Physik, Jungiusstrasse 11, 20355 Hamburg, Germany

A. M. MacLeod and W. A. Gillespie

School of Science and Engineering, University of Abertay Dundee, Bell Street, Dundee DD1 1HG, United Kingdom

G. Berden, G. M. H. Knippels, and A. F. G. van der Meer

FOM Institute for Plasma Physics “Rijnhuizen,” Edisonbaan 14, 3439 MN Nieuwegein, The Netherlands

(Received 10 September 2001; published 6 March 2002)

We report subpicosecond electro-optic measurements of the length of individual relativistic electron bunches. The longitudinal electron-bunch shape is encoded electro-optically on to the spectrum of a chirped laser pulse. The electron-bunch length is determined by analyzing individual laser-pulse spectra obtained with and without the presence of an electron bunch. Since the length of the chirped laser pulse can be easily changed, the electron bunch can be visualized on different time scales. This single-shot imaging technique is a promising method for real-time electron-bunch diagnostics.

DOI: 10.1103/PhysRevLett.88.124801

PACS numbers: 41.75.Ht, 41.60.Cr, 41.85.Ew, 42.65.Re



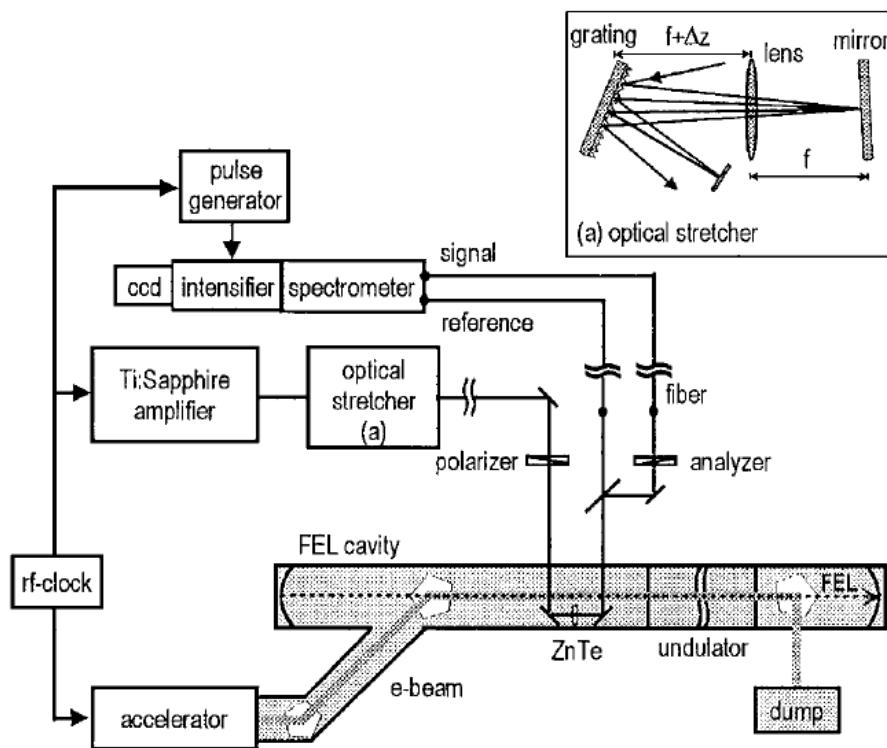


FIG. 1. Experimental setup for electron-bunch length measurements by electro-optic sampling with chirped optical pulses. The electron-bunch length is measured by using a ZnTe crystal placed inside the vacuum pipe at the entrance of the undulator. The inset (a) exhibits a simplified two-dimensional schematic of the optical stretcher. The lens and flat mirror are mounted on a linear translation stage (not shown). The focal length f of the lens is 200 mm.

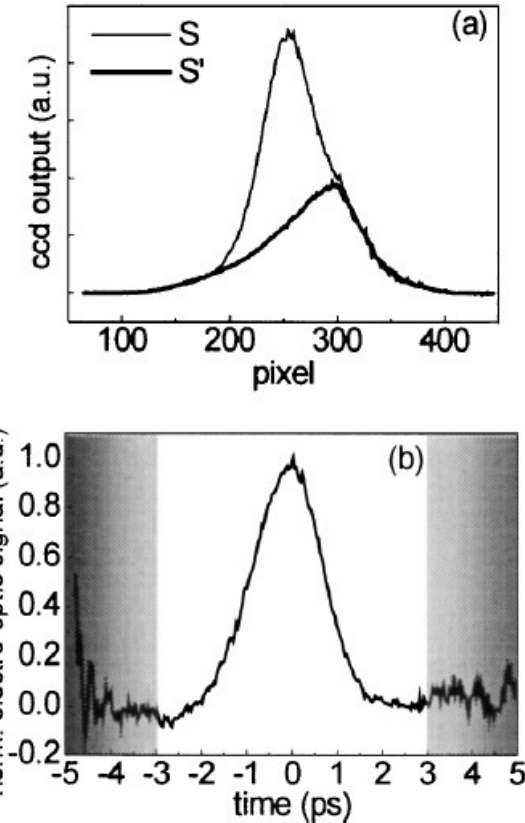
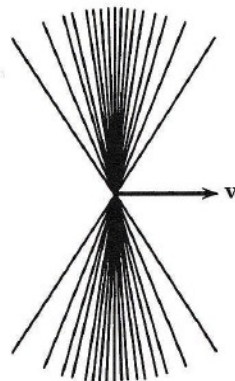


FIG. 2. Single-shot measurements of the electric field of individual electron bunches. (a) Raw data, single-shot chirped laser-pulse spectra S and S' . Spectrum S (thin solid line) is detected when the electron bunch and the chirped laser pulse overlap in time, while spectrum S' (bold solid line) indicates the spectrum that is measured when the laser pulse is 50 ps earlier than the electron bunch. (b) Electron-bunch length and shape obtained from the spectra as displayed in (a). The electron-bunch width is (1.72 ± 0.05) ps (FWHM). The leading edge of the electron bunch is to the right. The shaded areas indicate the regions of increased noise introduced by the correction for the wavelength dependent variations in intensity of the spectrum.



Thin-film lithium niobate modulators for non-invasive sensing of high-frequency electric fields

JOHN ROLLINSON,^{1,*} MONA HELLA,¹ SEYFOLLAH TOROGHI,² PAYAM RABIEI,² AND INGRID WILKE³ 

¹Department of Electrical and Computer Systems Engineering, Rensselaer Polytechnic Institute, 110 8th Street, Troy, New York 12180, USA

²Partow Technologies, LLC, 1487 Poinsettia Ave., Suite 119 Vista, California 92081, USA

³Department of Physics, Applied Physics, and Astronomy, Rensselaer Polytechnic Institute, 110 8th Street, Troy, New York 12180, USA

*Corresponding author: rollij2@rpi.edu

Received 16 October 2020; revised 3 December 2020; accepted 8 December 2020; posted 9 December 2020 (Doc. ID 412758); published 4 January 2021

We propose a non-invasive, large-bandwidth electro-optic (EO) detection scheme for high-frequency electric fields using thin-film lithium niobate Mach-Zehnder interferometers. Our proof-of-concept device is capable of detecting high-strength electric fields, such as those present in x-ray free electron lasers and linear accelerators. The proposed detection scheme utilizes an off-the-shelf C-band fiber optic continuous-wave laser and optical spectrum analyzer, which has a lower system cost and footprint compared to bulk-crystal-based schemes. Towards this objective, fabricated devices are characterized in the 1–40 GHz frequency range to estimate the detection threshold, detection bandwidth, and EO modulation strength. The characterized device exhibits a $0.13 \text{ V} \cdot \text{m}^{-1} \cdot \text{Hz}^{-1/2}$ normalized electric field sensitivity. By extrapolating the measured frequency response, it is expected that the characterized device will be able to detect free-space electric fields up to 150 GHz. © 2021 Optical Society of America

<https://doi.org/10.1364/JOSAB.412758>

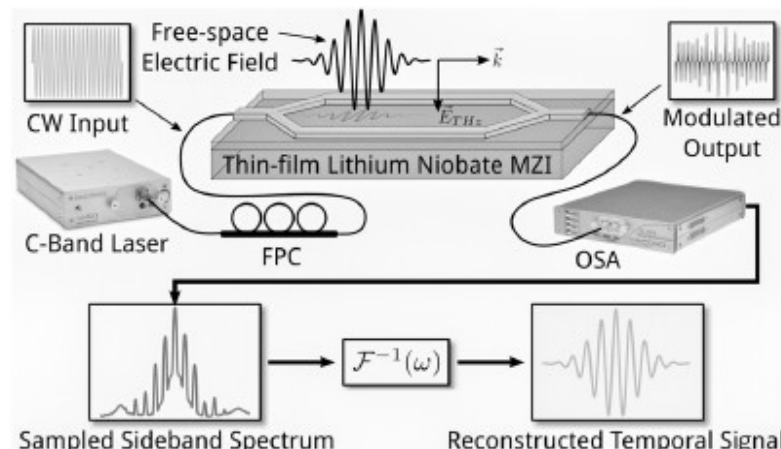


Fig. 1. Frequency-domain electro-optic detection scheme. Incident electric fields produce phase and amplitude modulation in an optical probe beam, which is captured in the frequency domain using an OSA.

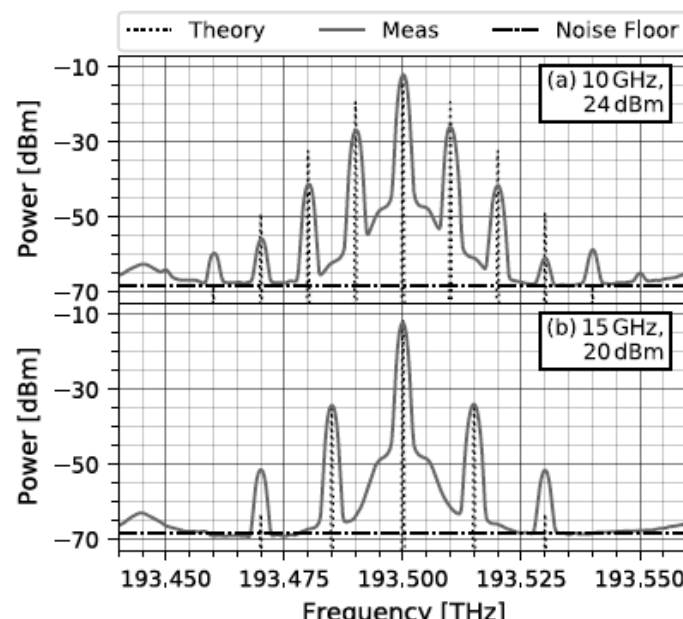


Fig. 3. Optical sideband spectra for (a) $f_{\text{RF}} = 10 \text{ GHz}$, $P_{\text{RF}} = 24 \text{ dBm}$ and (b) $f_{\text{RF}} = 15 \text{ GHz}$, $P_{\text{RF}} = 20 \text{ dBm}$. The elevated noise floor at the edges of the plot is due to the suppressed side modes of the laser (PPCL100). Note that the power level in (a) is 24 dBm, and hence the sideband ratios in this plot do not correspond to those in Fig. 5.

